Journal of Manufacturing Processes 88 (2023) 157–166

Contents lists available at ScienceDirect

Journal of Manufacturing Processes

journal homepage: www.elsevier.com/locate/manpro

Analytical modeling and experimental investigation of the particle scale energy absorption mechanism in laser-based directed energy deposition

Zhichao Liu [a,*], Manikanta Grandhi [a], Israt Zarin Era [a], Hong-Chao Zhang [b]

[a] Department of Industrial and Management Systems Engineering, West Virginia University, Morgantown, WV 26506, USA
[b] Department of Industrial, Manufacturing and Systems Engineering, Texas Tech University, Lubbock, TX 79409, USA

ARTICLE INFO

Keywords:
Directed energy deposition
Energy absorption
Analytical modeling
In-situ absorption measurement

ABSTRACT

Despite the tremendous application potential of advanced materials processing using laser-based directed energy deposition (DED), the reproducibility of metallic parts manufactured by this technology is limited due to the complex laser-material interactions during the material deposition process. Energy absorption and radiation by the powder stream attenuate the laser beam energy, thus affecting the actual energy delivered into the molten pool. The geometric and mechanical property irregularities in DED are directly related to the uneven energy input during continuous layers fabrication. This work reports a major advance in the particle scale energy absorption in DED as well as its relationship with the injected powder characteristics and process conditions (laser power, scanning speed, and powder feed rate). A novel simplified analytical model to analyze the effective absorptivity of continuous wave fiber laser is presented based on the stepwise heating method. The analytical model solution suggests that the effective absorptivity of the powder materials shows a slight decrease, from 8 % to 6 %, when the incident laser power increases from 250 W to 350 W. The model solution is verified using data from in-situ absorption measurements with a power meter. Theoretical calculations and experimental results showed that the energy absorption of high-density laser power in DED is not consistent, but negatively correlated with power input. Furthermore, we observed that lower powder temperature enhances energy absorption, which leads to the proposal that inverse bremsstrahlung absorption is the photophysical mechanism responsible for energy absorption by powder stream in DED additive manufacturing.

1. Introduction

Blown powder laser-based Directed Energy Deposition (DED) is an Additive Manufacturing (AM) technology to fabricate three-dimensional metal parts directly from raw materials with a layer additive method [1]. Due to the peculiar advantages of fabricating fully dense metal components and outstanding as-fabricated mechanical properties, DED is developing into a promising technology to boost industrial innovation in the metal components manufacturing processes, e.g., coatings for structural material [2], direct laser free-form fabrication [3–5] and high-added value components repair [6–8], etc. Despite the tremendous potential for high-performance materials processing using DED, the achievement of high-quality parts with good reproducibility has not yet been accomplished [9]. As documented in a report from a 2018 NSF Workshop on Accelerating AM toward Industrial Applications [10], although advances in process parameter optimization and in-situ monitoring have resulted in improvements in part quality [11,12], local defects and large variations in microstructure evolution contribute to large uncertainties in geometrical and mechanical properties [13].

Previous parameter fitting is always required to achieve optimal material properties, which means long and costly experimental work [14]. Although good mechanical and microstructural performance can be obtained by trial-and-error practices, the impact mechanism of process recipes on the part quality is still unclear [15–20]. It has been proved that microstructure evolution and mechanical responses of DED fabricated parts are highly dependent on the complex laser-material interactions above the molten pool, as shown in Fig. 1. When a laser beam strikes a high-density powder stream, the high-energy electrons are slowed down in the presence of the particles. At this moment, a small part of the absorbed energy is lost due to evaporative cooling and scattering, and another part of the laser energy is absorbed either in the vapor plume or in the plasma [21]. The absorbed energy is used for powder melting, and after powder absorption and radiation, the remaining beam energy reaches the substrate surface, generating the molten pool [22]. The energy transmitted into the molten pool

* Corresponding author.
E-mail address: zhichao.liu@mail.wvu.edu (Z. Liu).

https://doi.org/10.1016/j.jmapro.2023.01.030
Received 10 September 2021; Received in revised form 28 December 2022; Accepted 5 January 2023
Available online 26 January 2023

Nomenclature

Q_m	heat used to melt the particle before falling into the molten pool [J]
Q_a	heat absorbed by the particle [J]
Q_e	heat loss due to energy scattering [J]
Q_i	input laser energy density [J/mm^2]
α	energy absorption coefficient
r_p	radius of the particle [μm]
ε	emissivity of the materials
σ	Stefan-Boltzmann constant [Wm^{-2} K^{-4}]
T_p	end temperature of the particle [°C]
T_0	initial temperature of the powder [°C]
t	radiation time [s]
C_p	specific heat of the powder material [J/kg·K]
ρ	density of the powder material [g/cm^3]
N_p	total number of particles
Q_{scatt}	total scattered energy [J]
Q_{abs}	total energy absorption by the entire powder clouds [J]
P_L	power density [W/mm^2]
L'	length of the plasma [mm]
λ	Laser beam wavelength [mm]
P	laser power [W]
r	radius of the laser beam at the consolidation plane [mm]
d_c	distance from the consolidation plane to nozzle outlet [mm]
v_{pz}	vertical velocity of the powder [mm/s]
d_p	distance from the nozzle outlet to the beam center [mm]
r_0	radius of the nozzle outlet [mm]
(r, z)	cylindrical coordinate of the point P [mm]
v_p	velocity of the powder stream [mm/min]
r_s	powder stream radius [mm]
L	radius of the powder stream at the consolidation plane [mm]
$N(r,z)$	powder stream concentration [units/mm^3]
z	distance between the substrate surface and nozzle outlet [mm]
θ	inclination angle [° or deg]
P_0	actual laser power [W]
m	powder mass flow rate [g/min]
V	gas volumetric flow rate [L/min]
I_{in} & I_{out}	the incoming and the outgoing laser intensities [W/cm^2]
k_i	spatial damping rate of the laser energy by inverse bremsstrahlung

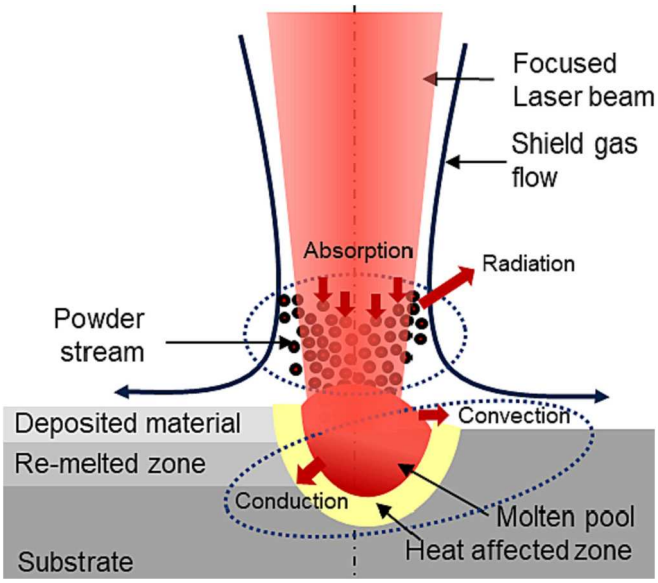

Fig. 1. Schematic diagram of the energy absorption and scattering in DED (Redrawn from [24]).

determines the microstructural evolution and therefore, needs to be well-controlled to produce a well-built part [23]. Energy absorption and radiation by the powder stream attenuate the laser beam energy, which determines the actual energy delivered into the molten pool. Therefore, to achieve the desired material properties and uncover the influence mechanism of the input parameters on material properties, the mechanism of energy absorption by the powder streams needs to be investigated.

Currently, limited studies have been reported on the energy absorption by metallic powders in additive manufacturing. The few studies that are available used either (i) optical method or (ii) stepwise heating (SWH) method for powder bed fusion (PBF) processes. The optical method indirectly infers the energy absorption of pre-deposited powders from light reflection measurement. The complexity of the experiment setup leads to a non-perfection of data collection and high cost [25]. SWH method assumes that the absorbed thermal energy is transferred to the heat of the powders, therefore, the energy absorptivity can be calculated by dividing the transferred energy, which is necessary to uniformly heat the powders to end temperature, with the total beam energy input [26]. Unlike the PBF processes, the powders delivered by the inert gases in DED cause unstable powder injection in the molten pool by the powder nozzle system. Although the laser-material interaction time in DED is longer than that of PBF processes, the number of particles involved is much smaller, therefore, it can be expected that the energy absorption in DED should be less than that of PBF processes. Usually, the energy absorption of the laser by metallic materials is considered constant, which is reasonable because it is either calculated or measured for polished clean metal plates. However, the energy absorption in DED involves a number of different physical phenomena when the metallic powders and substrate are heated by laser radiation. Laser light and powder surface interaction become non-stationary when the powders are melted [27]. It is extremely difficult to adequality interpret these complex effects through numerical modeling. Therefore, analytical modeling and experimental measurement are beneficial to illustrate the effective energy absorptivity for typical DED materials to allow accurate modeling and control of the laser-material interaction processes, thus achieving stable and repeatable process performances.

In this study, the particle scale energy absorption by the powder stream in the laser-based DED is investigated with both analytical modeling and in-situ experimental measurement. A novel simplified analytical model is built to theoretically calculate the effective energy absorption of the injected powders based on the SWH method. After presenting analytical modeling, changes in absorptivity under different laser power and powder temperature are presented. A high-resolution infrared (IR) camera is used to measure the end temperature of the powders after laser radiation. The particle scale energy absorption by the powder stream under various experimental conditions is presented and the effects of laser and scanning parameters as well as powder characteristics on the absorptivity are discussed. In the end, in-situ absorptivity measurement is performed by a power meter to validate the proposed model.

2. Materials and methods

2.1. Materials

Commercially available gas-atomized Inconel (IN) 718 powder (Carpenter Corp, Philadelphia, PA, USA) was used in this study, its chemical composition by weight is summarized in Table 1. The particle morphology under the scanning electron microscope (SEM) is shown in Fig. 2, indicating an approximating spherical geometry with an average diameter of 81.5 μm. Low carbon steel was used as the substrate material, and its surface was ground with abrasive papers to remove oxidation layers and then cleaned with acetone prior to deposition.

2.2. Analytical modeling

This section describes the bases of the proposed energy absorption model based on the SWH method. A single particle within the powder clouds is considered during analytical modeling. The proposed model was based on the following assumptions or facts:

(1) The powder stream below the deposition head follows Gauss distribution in the perpendicular direction to the nozzle centerline. In our previous study, the powder concentration is proved to follow Gauss distribution within the cross-section perpendicular to the particle velocity. And the spatial distribution of the powder particles depends on the powder's geometrical size and process conditions [31].
(2) Only the top half surface of the particle absorbs energy, and the intraparticle temperature gradient is neglected. The particles which are partly heated are fallen into the molten pool, whereas the powders that are not falling into the molten pool are lost due to collision either among the particles or with the substrate.
(3) Neglecting the gravity effect. This is reasonable because the laser-material interaction time is too short [32]. The velocity of the powder is considered the same as the speed of carrier gas at the nozzle outlet [33].
(4) The laser beam energy is uniformly distributed and there is no divergence or convergence in the power-powder interaction zone.
(5) The powder particles are considered spherical and their projection on the consolidation plane is approximately a circle.
(6) Neglecting the laser refraction and heat convection among the powders due to their weak effect.

According to the energy balance law, the heat used to melt the particle before entering the molten pool (Q_m) can be expressed as Eq. (1).

$$Q_m = Q_a - Q_e = \alpha\pi r_p^2 Q_i - Q_e \tag{1}$$

where, Q_a is the heat absorbed by the particle [J], Q_e is the heat loss due to energy scattering [J], Q_i is the input laser energy density [J/mm^2], α is the energy absorption coefficient (the ratio of the absorbed energy to the incident laser beam energy) of the particle, r_p is the radius of the particle (mm). According to the Stefan-Boltzmann Law, the energy loss due to scattering during material deposition can be expressed as Eq. (2):

$$Q_e = 4\pi r_p^2 \varepsilon\sigma\left(T_p^4 - T_0^4\right)t \tag{2}$$

where, ε is the emissivity of the materials ($\varepsilon < 1$), indicating a measurement of efficiency in which a surface emits thermal energy. σ is the Stefan-Boltzmann constant, T_p is the end temperature of the particle [°C], T_0 is the initial temperature of the powder [°C], and t is the radiation time [s]. According to the SWH method, Q_m can also be calculated with Eq. (3):

$$Q_m = \left(C_p\rho\frac{4}{3}\pi r_p^3\right)\cdot\left(T_p - T_0\right) \tag{3}$$

In Eq. (3), C_p is the specific heat of the powder material (J/kg·K), ρ is the density of the powder material (g/cm^3). Combining Eqs. (1)–(3), α can be deduced, as shown in Eq. (4):

$$\alpha = \frac{4\pi r_p^2\varepsilon\sigma\left(T_p^4 - T_0^4\right)t + \left(C_p\rho\frac{4}{3}\pi r_p^3\right)\cdot\left(T_p - T_0\right)}{\pi r_p^2 Q_i} \tag{4}$$

Finally, the total energy absorption by the entire powder clouds (Q_{abs}) can be calculated by multiplying the total number of particles (N_p) within the power-powder interaction zone with the energy absorbed by a single particle, as calculated in Eq. (5).

$$Q_{abs} = Q_a N_p = \alpha\pi r_p^2 Q_i N_p \tag{5}$$

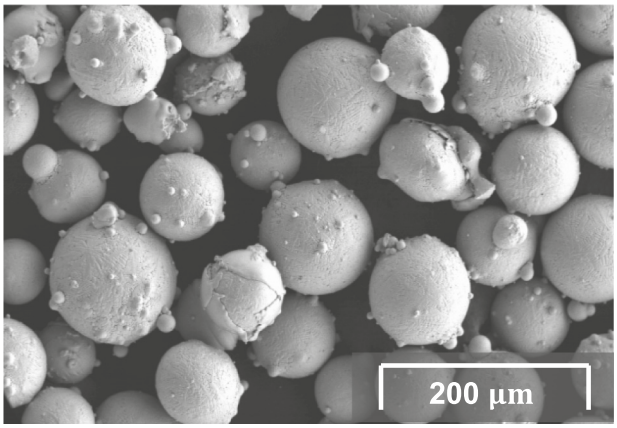

Fig. 2. Particle morphology of IN 718.

2.3. Model resolution method

2.3.1. Quantification of laser energy input (Q_i)

An Optomec LENS 450 system (Optomec, Albuquerque, NM, USA) was used for part fabrication. The system has a 100 mm cubed working volume and a 400 W IPG fiber laser. The four-jet nozzles inject the powders and guide them to a converging point at the deposition plane. To prevent oxidation and ensure there is no impurity pick-up during deposition, the LENS process is housed in a chamber that is purged with argon. To calculate the input laser energy (Q_i, J/mm^2), the travel time of the particle from the nozzle outlet to the consolidation plan needs to be considered. A cross-section of the powder stream below the deposition head is shown in Fig. 3.

Based on the geometrical relationship, laser energy density (Qi, J/mm^2), and radiation time (t) can be calculated with Eq. (6).

$$Q_i = P_L t = P_L\frac{d_c}{v_{pz}} = \frac{Pd_c}{\pi r^2 v_{pz}} \tag{6}$$

where P_L is the laser beam power density (W/mm^2), P is the laser power (W), r is the radius of the laser beam (mm) at the consolidation plane, d_c

Table 1
Chemical composition of Inconel 718 (% weight).

C	Mn	Si	P	S	Cr	Ni + Co	Mo	Nb + Ta	Ti	Al	B	Cu	Fe
0.10	0.35	0.35	0.015	0.015	19.00	52.50	3.05	5.25	0.90	0.60	0.004	0.15	Bal.

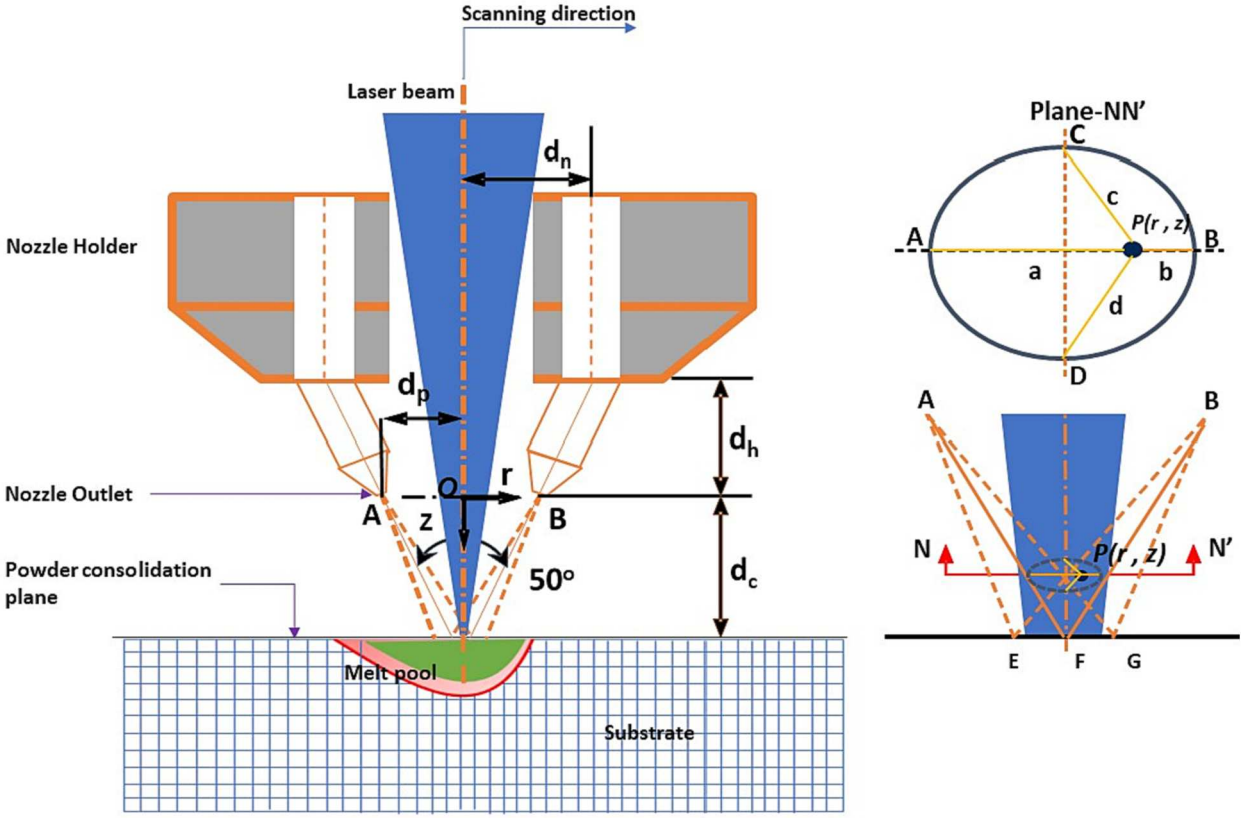

Fig. 3. Cross-section of the powder stream under the deposition nozzle (Redrawn from [31]).

is the distance from the consolidation plane to the nozzle outlet (mm), v_{pz} is the vertical velocity of the powder (mm/s). Based on assumption Eq. (3), v_{pz} can be calculated with Eq. (7), where d_p is the distance from the nozzle outlet to the beam center (mm), r_0 is the radius of the nozzle outlet (mm).

$$v_{pz} = \frac{Vd_c}{4\pi r_o d_p \sqrt{d_c^2 + d_p^2}} \tag{7}$$

2.3.2. End temperature of the powder stream (T_p)

When the metal powders are ejected out of the nozzles, the high-pressure argon gas provides four high-speed powder streams. The powders travel through the laser beam and arrive at the consolidation plane in about 10 milliseconds, during which laser radiation of the powders occurs. After laser radiation, the end temperature of the powders equals the molten pool surface temperature when the powders contact the molten pool. To collect the real-time temperature of the powder stream after laser radiation, a high-resolution (768 × 576 pixels) infrared camera (PYROVIEW 768 N, DIAS Inc., Dresden, Germany) was placed inside the system chamber, targeting the powder converging point. The camera has a high-dynamic CMOS sensor with a sensitivity of 0.8 to 1.1 μm and a sampling rate of 25 Hz. The experimental setup for temperature measurement is shown in Fig. 4 [34].

2.3.3. Modeling of the powder stream concentration

Powder concentration out of the injection nozzle depends on nozzle types and process conditions. Generally, three types of nozzles are used in DED, including coaxial nozzle, three-jet nozzle, and four-jet nozzle. For the four-jet exit nozzle, the powders are injected with four outlets and converged at a point below the deposition head. This study attempts to establish the energy absorption model of this type of nozzle and derive the particle scale energy absorption mechanism. The N (r, z) (units/mm^3) out of the four-jet exit nozzles is referred from the

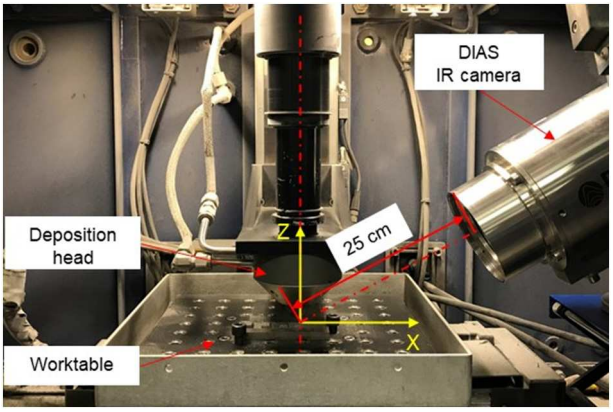

Fig. 4. Experimental set up for end temperature measurement.

previously established analytical model by the authors [31], as expressed in Eqs. (8)–(12):

$$N(r,z) = \frac{M_A + M_B + M_C + M_D}{\rho \frac{4}{3}\pi r_p^3 v_p} = \frac{\frac{m}{\pi r_s^2}\left[exp\left(\frac{-2a^2}{r_s^2}\right) + exp\left(\frac{-2b^2}{r_s^2}\right) + exp\left(\frac{-2c^2}{r_s^2}\right) + exp\left(\frac{-2d^2}{r_s^2}\right)\right]}{\rho \frac{4}{3} r_p^3 \frac{V}{4\pi r_0 d_p}} \tag{8}$$

$$a = \left|\left(\frac{d_c - z}{d_c}\right) d_p - r\right| \tag{9}$$

$$b = \left|\left(\frac{d_c - z}{d_c}\right) d_p + r\right| \tag{10}$$

$$c = d = \sqrt{r^2 + (r+a)^2} \tag{11}$$

$$r_s = \frac{z}{d_c}(L - r_0) + r_0 \tag{12}$$

where, r, and z are the cylindrical coordinates of the point P (mm) within the laser-material interaction zone, M_A, M_B, M_C, and M_D are the mass flow rate of the powders under nozzles A, B, C, and D (g/mm^{2}s), v_p is the velocity of the powder stream (mm/min). L is the radius of the powder stream at the consolidation plane (mm), L = 2.267 mm. The powder stream radius (r_s) (as a function of z) can be expressed as Eq. (12) according to the triangle similarity theorem. a, b, c, and d are the distances of the point P (r, z) to the center line of each of the powder streams, as is shown in Fig. 3. E.g., AF and BF represent the center line of the powder stream out of nozzles A and B.

2.3.4. Design of experiment

The thermophysical properties of the IN 718 powder and known parameters were given in Table 2. Multiple layers and single-track specimens were built to investigate the energy absorption by the powders under various process conditions. Shielding and carrier gas consist of argon with a flow rate of 6 L/min. The laser power values were 250 W, 275 W, 300 W, 325 W, and 350 W. The scanning speeds were 5 mm/s, 7 mm/s, and 9 mm/s, resulting in five substrates with fifteen single walls. The powder feeding rate for all experiments was 4 g/min.

Material's emissivity (ε) is subject to the wavelength and the temperature, and it can also be influenced by the transient surface appearance. The emissivity value of IN 718 increases proportionally with increasing temperature [35]. In this work, the authors inferred the emissivity of IN 718 as 0.58 under the melting state (above 1650 °C) based on the literature [35].

3. Results and discussion

3.1. End temperature of powder streams above the molten pool

Fig. 5 (a) shows a measured molten pool image and temperature data for a thin wall specimen with eight layers. The maximum temperature is found near the center of the molten pool, reaching up to 2000 °C. The edge of the molten pool is irregular because some powders located at the edge of the molten pool are partially melted. The end temperature of the powders collected during the first layer deposition is shown in Fig. 5 (b), indicating that the average temperature at this experimental condition is 1593 °C with a fluctuation ($\triangle$T) <100 °C, indicating a good consistency. Repeating the end temperature experiments, and substituting measured T_p into Eq. (4), can yield the energy absorption coefficient of the Inconel 718 under different input parameters.

3.2. Powder stream concentration

The powder stream concentration model is simulated with Matlab software with the known process variables summarized in Table 2. When m = 4 g/min, the simulation result of N (r, z) is shown in Fig. 6, indicating that the powder concentration follows Gaussian distribution within 2 mm above the consolidation plane. At the focal plane (z = 9.525 mm), the powder concentration reaches the maximum (N = 4.7918 units/mm^3) at the center position of the deposition head ($r = 0$, z = 9.525) and decreases when r is getting larger. From the X-Z or Y-Z views in the vertical direction, the maximum powder flow concentration (N_{max} = 4.9252 units/mm^3) occurs at the center position above the consolidation plane ($r = 0$, $z = 0.5$).

Table 2
Physical properties of Inconel 718 and known parameters.

Physical properties of IN 718		Parameters/constant	
ρ (g/cm^3)	8.15	d_p (mm)	6.4
r_p (μm)	40.75	d_c (mm)	9.525
C_p(J/g· °C)	0.435	r (mm)	0.45
T_0 (K)	296.15	σ(Wm^{-2} K^{-4})	5.670373 × 10^{-8}
ε	0.58	r_0 (mm)	1.2

During the DED process, powders are blown through the nozzle into a molten pool, therefore the powders within the laser beam are deposited on the substrate, while the particles outside the laser beam are blown away by the shielding gas flow. The total number of particles (N_p) within the laser-material interaction zone can be calculated by taking triple integrals of the powder concentration with (θ, r_1, z) under cylindrical coordinates. N_p can be calculated by Eq. (13):

$$N_p = 4\int_0^z \int_0^r \int_0^{\frac{\pi}{2}} \theta N(r,z) d_\theta d_r d_z \tag{13}$$

where z is the distance between the substrate surface and the nozzle outlet, r is the radius of the laser beam (r = 0.45 mm) at the consolidation plane, and θ is the inclination range from 0 to $\frac{\pi}{2}$. N_p equals 30.2563 units (m = 4 g/min), which means about 30 particles are within the laser-material interaction zone in unit time.

3.3. Energy absorption/scattering by the powder streams

The energy absorption of the powders under laser radiation depends on several parameters, including laser wavelength, material property, ambient gas, and surrounding temperature, etc. [25]. For the DED process of IN 718, the relationship between energy absorption rate, laser power, and end temperature of the powder stream is illustrated in Fig. 7. The result shows that the energy absorption coefficient (α) is not constant, and it depends on the laser power and powder temperature during material deposition. There is a negative relationship between the power input and the energy absorption coefficient. The power absorption rate decreases from 7.4 % to 6.0 % when the laser power increases from 250 W to 350 W.

The total energy absorbed by the entire powder stream, Q_{abs} was calculated by multiplying the energy absorption coefficient and the total number of the powders (N_p) within the laser-material interaction region, as shown in Eq. (5). Similarly, total scattered energy, Q_{scatt} was calculated by multiplying the energy scattered by a single particle (Q_e), and N_p. The calculated energy absorption and scattering under various laser power inputs during DED are shown in Fig. 8. Although the energy absorption rate (α) decreases with the increase of the laser power, energy absorption by the entire powder stream increases when the laser power increases from 250 W to 350 W, indicating the increasing laser energy input (Q_i) had a greater effect on powder stream energy absorption. Fig. 6 also indicates the end temperature of the entire powder stream increases with the laser power input, this is the reason that can explain total scattered energy increases with the increase of the laser power.

3.4. Effects of process conditions on the energy absorption

To illustrate the energy absorption under different additive manufacturing (AM) processes, the energy absorption rate at the laser power of 300 W in DED was compared with previous studies. The result is summarized in Table 3. Based on the data in Table 3, the energy absorption of the powders in AM is not only related to process types but also related to material types and characteristics as well as process parameters, such as powder feeding rate. Apparently, energy absorption varies for different material types, because of the difference in absorption mechanisms exhibited by the different materials. The optical response of metal is dominated by the electrons located in states close to the fermi level, referred to as free electrons. Different laser sources (e.g., Nd-YAG versus CO_2) may cause different energy absorption, even though the AM process and powders are the same. This phenomenon can

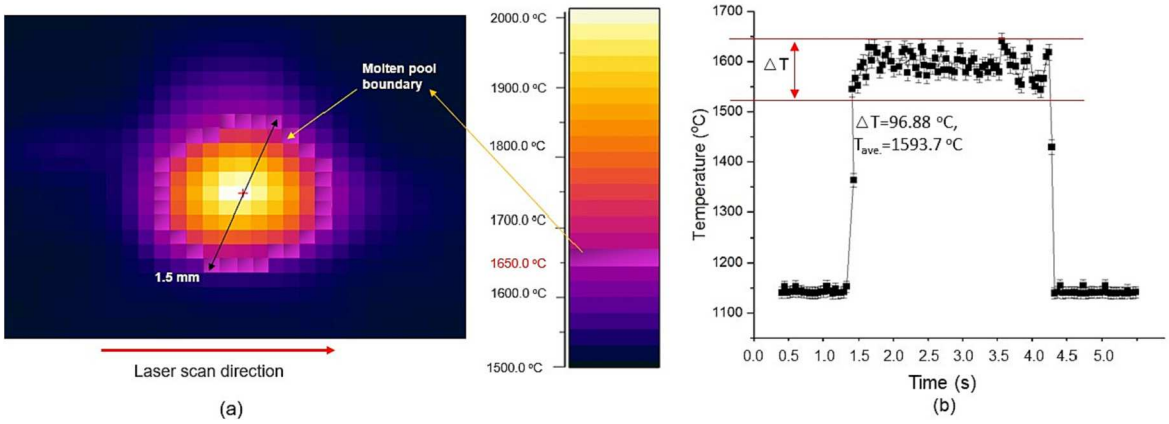

Fig. 5. Result of end temperature measurement. (a) Temperature profile, (b) End temperature of the powders ($P = 250$ W, $v = 7$ mm/s).

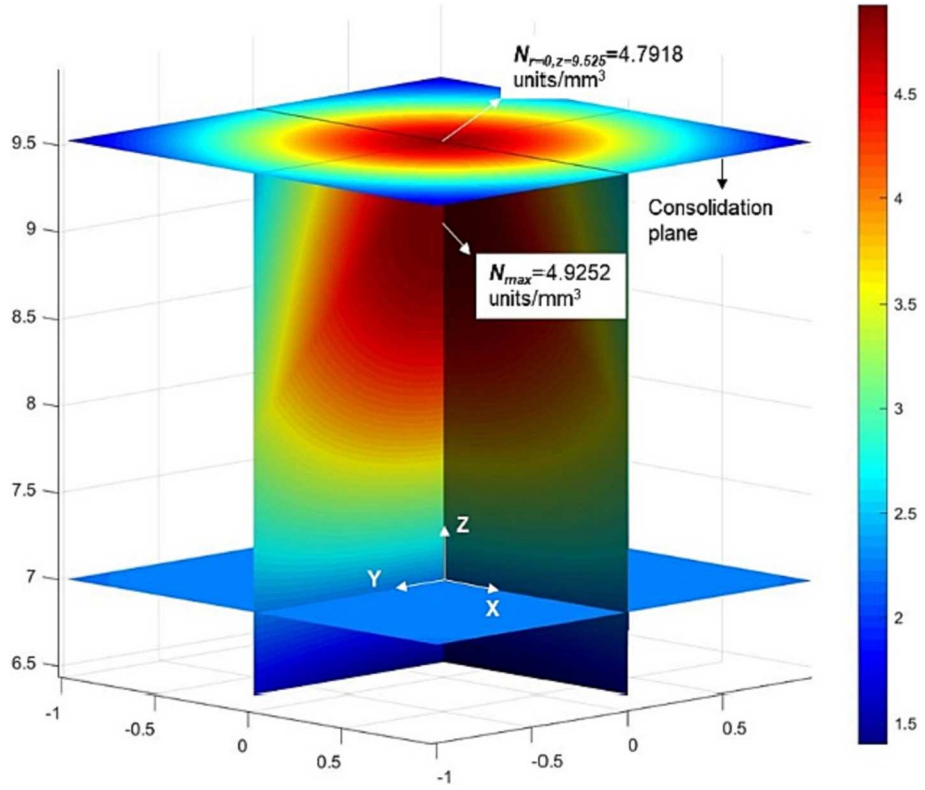

Fig. 6. Simulation result of the powder flow concentration of four-jet deposition nozzle.

be explained by the density of the plasma and its related oscillation frequency. At a high pulse frequency, more material is ablated, leading to a higher plasma density [41–44]. Therefore, a higher amount of the still incoming energy is absorbed. In addition, laser absorption is governed by particle size morphology, distribution, and surface topology [28]. Within the bulk powder, the lower median particle sizes lead to an increase in energy absorption for the multiple reflections caused by laser radiation [29,30]. Typically, the mean particle sizes in DED are quite higher than in the PBF process which is evidently shown in Table 3. It is also proved that the PBF process (e.g., SLS) and pre-deposited laser cladding has higher power efficiency compared with that of the coaxial and side injection DED process. As mentioned earlier, the powders delivered in the DED process cause unstable powder injection in the molten pool by the coaxial or side powder nozzle system. Although the laser-material interaction time in DED is longer than that of PBF processes, the number of particles involved is much smaller, therefore, the energy absorption in DED should be less than that of PBF processes [27].

Energy absorption by the entire powder stream is directly related to the total number of particles (N_p) within the laser-material interaction zone, as shown in Eq. (5). Eq. (8) suggests that N_p not only depends on the nozzle geometrical sizes, including dp, dc, L, and r_o, but also the input variables, including m, V, and r_p. To investigate the sensitivities of energy absorption with various process conditions, a scenario analysis was conducted.

To investigate the relationship of energy absorption with input variables, a sensitivity study is performed at the laser power of 300 W. Three different levels of m, V, and r_p are defined: $m = 2$, 3, and 4 g/min; $V = 5$, 6, and 7 L/min; $r_p = 30$, 40, and 50 μm. The powder concentration below the deposition head (N_p) under different experimental conditions

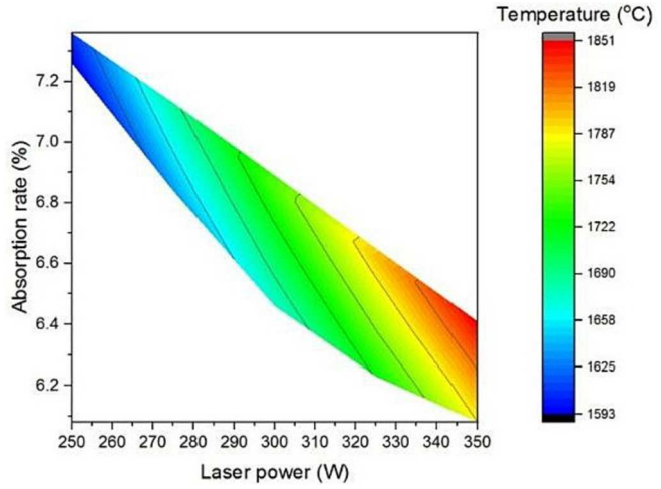

Fig. 7. Relationship between the laser power input and energy absorption coefficient.

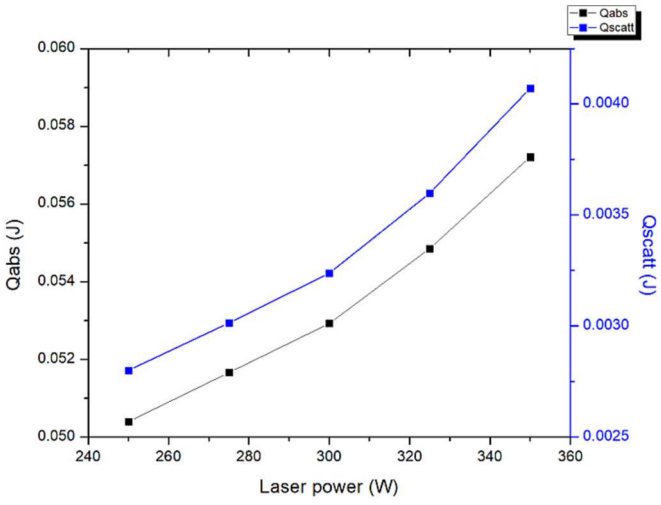

Fig. 8. Results of the total energy absorbed/scattered by the entire powder stream.

can be calculated with Eq. (5). Substituting N_p into Eq. (8) can yield the results of energy absorption at different scenarios, the result is shown in Table 4. Sensitivity analysis results suggest that the total energy absorption (Q_{abs}) increases proportionally with the increase of the powder feeding rate, while decreasing with the increase of the gas flow rate and powder size. This can be explained by the relationship between N_p and input variables. Eq. (5) indicates that N_p is positively related to powder feeding rate, and negatively related to particle size, which means higher powder concentration appears at higher powder feeding and smaller particles. While with the increasing gas flow rate, the velocity of the powders increases, and there will be fewer powders appearing in the laser-material interaction zone in the unit space.

4. Experimental validation

4.1. Experimental set-up design

To verify the proposed energy absorption measurement model, a power meter (FL400A-BB-50, Ophir, North Logan, USA) is used to measure the real-time power output before and after the powder injection. The power meter has a measurement range of 300 mW–500 W with 88 % absorption. The response time is 4 s with 3 % accuracy. The

Table 3
Comparison of the material energy absorption in AM processes.

AM process	Material	Laser source	Particle size (diameter: μm)	Powder feeding (g/min)	Absorption rate (%)
Selective laser sintering [25]	Ni-alloy	Nd-YAG (pulsed, λ = 1.06 μm)	<50	N/A	64
		CO_2 (CW, λ = 10.6 μm)		N/A	72
Laser cladding (Pre-deposited) [36]	Cu-alloy	CO_2 (CW, λ = 10.6 μm)	10–150	N/A	42
Laser cladding (Coaxial) [37]	Ni-alloy	Nd-YAG (pulsed, λ = 1.06 μm)	100	4	8.18
Laser cladding (Coaxial) [38]	N/A	CO_2 (CW, λ = 10.6 μm)	80	4	5.33
Laser cladding (Side injection) [39]	Co-alloy	CO_2 (CW, λ = 10.6 μm)	50	5	20
Laser cladding (Side injection) [40]	Co-alloy	CO_2 (CW, λ = 10.6 μm)	80	12	10
DED	Ni-alloy	Fiber (CW, λ = 1.06 μm)	81.5	4	6.46

Note: N/A means Not Available.

Table 4
Results of sensitivity analysis of the input variables.

	N_p	Q_{abs} (J)
m (g/min)		
2	15	0.026
3	22	0.038
4	30	0.053
V (L/min)		
5	36	0.063
6	30	0.053
7	25	0.044
r_p (μm)		
30	76	0.134
40	32	0.056
50	16	0.028

experimental setup is shown in Fig. 9. The power meter is placed under the four-jet exit nozzle. To ensure the energy can be absorbed by the entire powder stream, and to avoid the powders being deposited on the sensor, a safe distance is set up (25 mm) between the power meter and nozzle outlet. An anti-reflection BK7 glass (wavelength: 1064 nm) is placed upper the meter to protect it from damage by the powders from the upper area. Another function of the glass is to reduce the reflection of laser radiation. Also, an air filter is used to wrap the meter to protect it from damage by the powders from the surrounding area. A data transmitter and StarLab software (v3.31, Ophir, North Logan, USA) are used to record and analyze the actual power output.

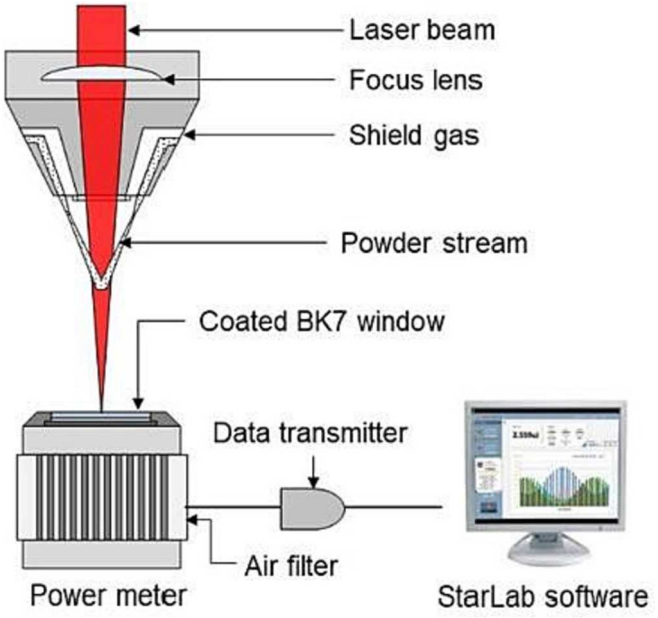

Fig. 9. Experimental setup for model verification.

4.2. Validation under controlled experiment

In the beginning, the power meter is used to calibrate the actual power output. With the five laser power levels mentioned in Section 2.3.4, the measured actual laser power (P_0) is 183 W, 206 W, 226 W, 245 W, and 268 W when the original laser power setup is 250 W, 275 W, 300 W, 325 W, and 350 W respectively. Next, the deposition head remains steady, then the laser is turned on and maintained for 30 s without the powder (In 718) injection. The power output with powder injection is recorded as P_0. After 30 s, the powder feeding starts, and keeps the laser running for another 30 s. The power output with powder injection is recorded as P_1. Totally, five datasets were obtained under various power inputs. Fig. 10 shows the collected actual power output with/without powder injection at a laser power of 250 W.

In Fig. 10, the powder injection starts at point A, then the power after the powder injection decreases from 183 W (P_0) to 175 W (P_1). Neglecting the powder reflection, the difference between P_0 and P_1 is the energy absorbed by the powder streams. The energy absorption coefficient (α, $\alpha = (P_0 - P_1) / P_0$) at different power inputs can be calculated by repeating the power output measurement experiments. The result is shown in Fig. 11. The experimental value of energy absorption by the powder stream decreases with the increase of the laser power, which is consistent with simulation results and proves the reliability of the proposed energy absorption model The experimental value is a little bit less than the theoretical value, there are two reasons: (1) Part of the laser energy is reflected by the powder stream, and (2) Secondary absorption occurs because of phonons formation due to surface imperfections when the powder particles are blown back to the laser beam area by the carrier gas [45–48].

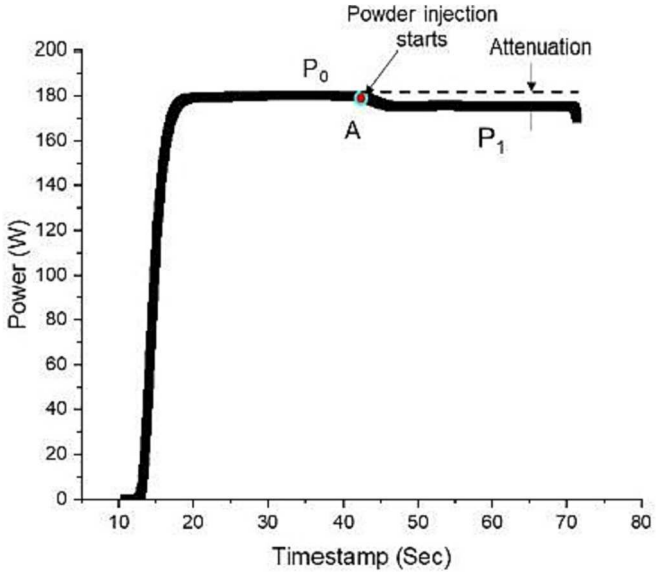

Fig. 10. Result of real-time power output ($P = 250$ W).

4.3. Energy absorption mechanism in DED

The values for the energy absorption coefficients shown in Table 4 indicate that the energy absorption in DED is in accordance with the inverse bremsstrahlung absorption mechanism (IBAM) [49]. IBAM is the result of the interaction between laser and powder materials, which leads to many important physical phenomena. When a focused laser beam hits the powder streams, the laser photon energy is transferred to the plasma through the electron-ion collision, during which the radiation energy is imparted to the powders [50]. Based on IBAM, Once the laser energy is transformed into plasma, the absorption coefficient (α) can be calculated by Eq. (14) [51]:

$$\alpha = \frac{I_{in} - I_{out}}{I_{out}} = 1 - exp(-2k_i L') \tag{14}$$

where I_{in} and I_{out} are the incoming and the outgoing laser intensities (W/cm^2). k_i is the spatial damping rate of the laser energy by inverse bremsstrahlung, L' is the length of the plasma (mm). Eq. (14) suggests that there is an inverse correlation between energy absorption and the length of plasma generated in the DED process. With the increase of the electron temperature, the electron density decreases, and at the same time, the length of plasma decreases, then, the energy absorption decreases by increasing the electron temperature. This can explain the relationship between the end temperature of the powders and energy absorption in Fig. 7. The energy absorption by the powder stream is also related to the particle's velocity distribution. Considering the particle velocity distribution follows Maxwellian distribution or Kappa distribution, with different k, the variation of α with respect to laser intensity is shown in Fig. 12.

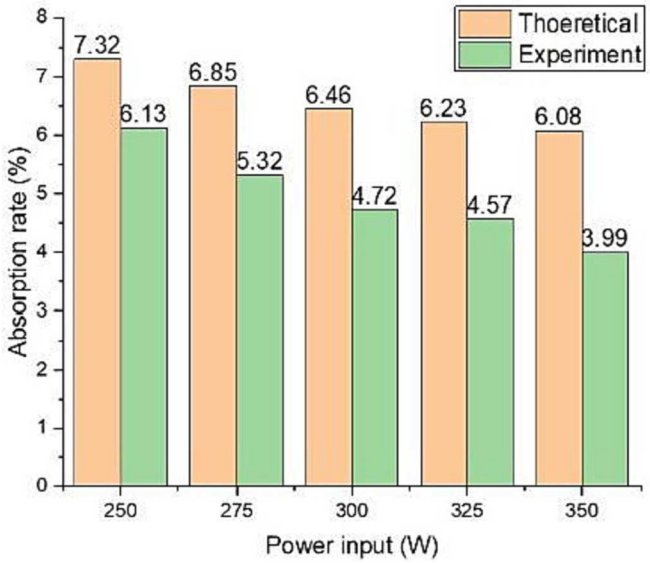

Fig. 11. Comparison of theoretical and experimental energy absorption result.

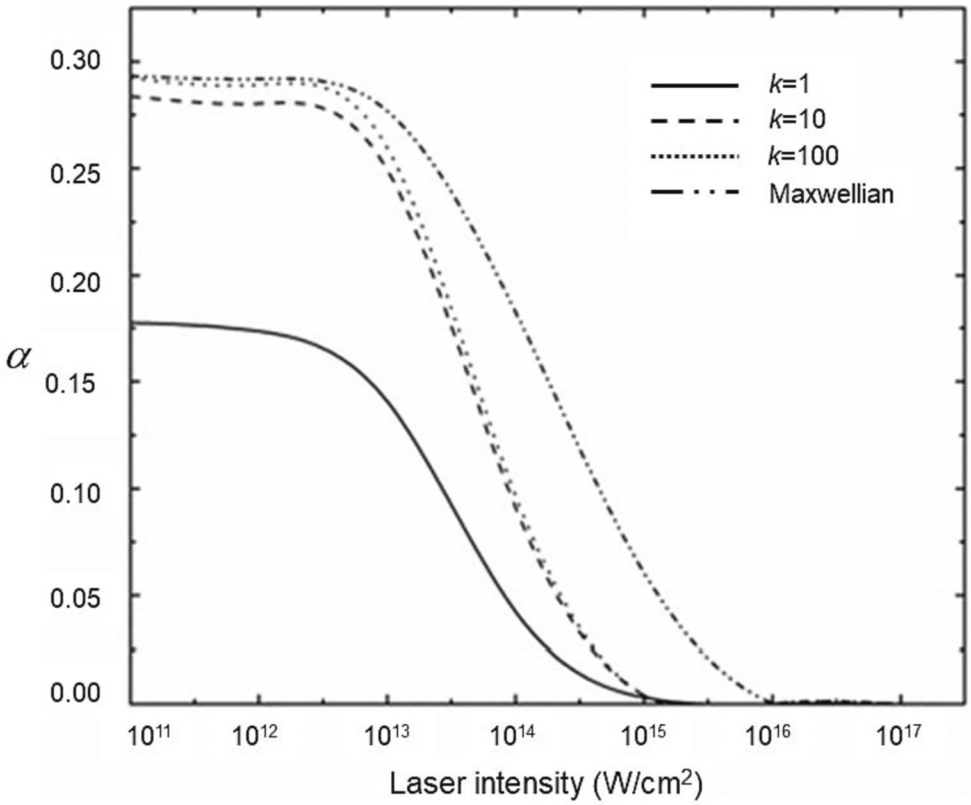

Fig. 12. Variation of energy absorption with respect to laser intensity (Redrawn after [26]).

As mentioned earlier, the microstructural evolution and material property in DED are closely related to the energy transmitted into the molten pool. While the energy input to the molten pool is hardly constant due to the variations in energy absorption. This can also explain the variation of the molten pool temperature in Fig. 5b. It can be reasonably inferred that repeatable part quality occurs when the laser energy is controlled to meet the energy demand of the molten pool. Therefore, the findings of this study can provide a basis to understand the variations in part quality under different processing conditions. It can also be used to build the energy requirement model of the molten pool, with which the inherent relation and regularity between the initial parameters and corresponding mechanical behaviors can be revealed.

It should be noted that the energy absorption of the powders varies with the changes in power density and free electron distribution. Because the free electron distribution is inherently related to powder velocity and spreading behavior. Therefore, it is rather important to identify powder spreading mechanisms to further unveil the energy absorption regularity. Future research will focus on the relationship of free electron distribution with powder spreading behavior as well as the energy absorption in laser-based DED.

5. Conclusions

In this study, the power absorption by the powder stream is numerically calculated and experimentally validated. The energy absorption coefficient of IN 718 under different laser energy inputs is calculated based on the stepwise heating method. The experimental method with a power meter is used to verify the energy absorption coefficient. The proposed model can be used to reveal the laser-material interaction mechanism as well as to figure out the source of variations in part qualities. The main findings can be drawn as follows:

(1) There is a negative relationship between the powder temperature and the energy absorption coefficient. The energy absorption rate of the powder is not constant in DED, ranging from 6 % to 8 % for IN 718 deposition. The power absorption rate decreases with increasing laser power.
(2) The variation of power absorption is in accordance with the inverse bremsstrahlung mechanism. With the increase of the electron temperature, the electron density decreases, and at the same time, the length of plasma decreases, then, the energy absorption decreases by increasing the electron temperature.
(3) Due to the energy reflection by the powder stream and the occurrence of secondary absorption, the experimentally measured energy absorption is less than the numerically calculated results.

Declaration of competing interest

The authors declare that they have no known competing financial interests or personal relationships that could have appeared to influence the work reported in this paper.

Acknowledgments

This material is based upon work supported by the National Science Foundation under Grant No. 2119654. Any opinions, findings, and conclusions or recommendations expressed in this material are those of the author(s) and do not necessarily reflect the views of the National Science Foundation.

References

[1] Standard ASTM. Standard terminology for additive manufacturing technologies. ASTM International; 2012. F2792-12a.
[2] Ramiro P, Ortiz M, Alberdi A, Lamikiz A. Characteristics of Fe-based powder coatings fabricated by laser metal deposition with annular and four stream nozzles. Procedia CIRP 2018;74:201–5.

[3] Reichardt A, Dillon RP, Borgonia JP, Shapiro AA, McEnerney BW, Momose T, Hosemann P. Development and characterization of Ti-6Al-4V to 304L stainless steel gradient components fabricated with laser deposition additive manufacturing. MaterDes 2016;104:404–13.
[4] Qiu C, Ravi GA, Dance C, Ranson A, Dilworth S, Attallah MM. Fabrication of large Ti–6Al–4V structures by direct laser deposition. J Alloys Compd 2015;629:351–61.
[5] Keist JS, Palmer TA. Role of geometry on properties of additively manufactured Ti-6Al-4V structures fabricated using laser based directed energy deposition. MaterDes 2016;106:482–94.
[6] Kaierle S, Overmeyer L, Alfred I, Rottwinkel B, Hermsdorf J, Wesling V, Weidlich N. Single-crystal turbine blade tip repair by laser cladding and remelting. CIRP JManufSciTechnol 2017;19:196–9.
[7] Petrat T, Graf B, Gumenyuk A, Rethmeier M. Laser metal deposition as repair technology for a gas turbine burner made of Inconel 718. PhysProcedia 2016;83:761–8.
[8] Kumar LJ, Nair CK. Laser metal deposition repair applications for Inconel 718 alloy. MaterTodayProc 2017;4(10):11068–77.
[9] Sames WJ, List FA, Pannala S, Dehoff RR, Babu SS. The metallurgy and processing science of metal additive manufacturing. Int Mater Rev 2016;61(5):315–60.
[10] Xiong W, Bedewy M, Kuhn H, Elwany A, Pei Z. Report of NSF workshop on accelerating NSF research in additive manufacturing toward industrial applications. 2018. Pittsburgh, PA.
[11] Soshi M, Odum K, Li G. Investigation of novel trochoidal toolpath strategies for productive and efficient directed energy deposition processes. CIRP Ann 2019;68(1):241–4.
[12] Schmidt M, Kolleck R, Grimm A, Veit R, Bartkowiak K. Direct laser deposition of Cu alloy on forming tool surfaces—process window and mechanical properties. CIRP Ann 2010;59(1):211–4.
[13] Sames WJ, List FA, Pannala S, Dehoff RR, Babu SS. The metallurgy and processing science of metal additive manufacturing. Int Mater Rev 2016;61(5):315–60.
[14] Saboori A, Bosio F, Librera E, de Chirico M, Biamino S, Lombardi M, Fino P. Accelerated process parameter optimization for directed energy deposition of 316L stainless steel. In: Proceedings of the Euro PM2018 Congress Exhebition, Bilbao, Spain; 2018. p. 14–8.
[15] Tabernero I, Lamikiz A, Martínez S, Ukar E, Figueras J. Evaluation of the mechanical properties of Inconel 718 components built by laser cladding. Int J Mach Tool Manuf 2011;51(6):465–70.
[16] Zhao X, Chen J, Lin X, Huang W. Study on microstructure and mechanical properties of laser rapid forming Inconel 718. Mater Sci Eng A 2008;478(1–2):119–24.
[17] Zhong C, Pirch N, Gasser A, Poprawe R, Schleifenbaum JH. The influence of the powder stream on high-deposition-rate laser metal deposition with Inconel 718. Metals 2017;7(10):443.
[18] Parimi LL, Ravi GA, Clark D, Attallah MM. Microstructural and texture development in direct laser fabricated IN718. Mater Charact 2014;89:102–11.
[19] Tian Y, McAllister D, Colijn H, Mills M, Farson D, Nordin M, Babu S. Rationalization of microstructure heterogeneity in Inconel 718 builds made by the direct laser additive manufacturing process. MetallMaterTransA 2014;45(10):4470–83.
[20] Stevens EL, Toman J, To AC, Chmielus M. Variation of hardness, microstructure, and laves phase distribution in direct laser deposited alloy 718 cuboids. MaterDes 2017;119:188–98.
[21] Allmen MV, Blatter A. Laser-beam interactions with materials: physical principles and applicationsVol. 2. Springer Science & Business Media; 2013.
[22] Tabernero I, Lamikiz A, Martinez S, Ukar E, De Lacalle LL. Modelling of energy attenuation due to powder flow-laser beam interaction during laser cladding process. J Mater Process Technol 2012;212(2):516–22.
[23] Liu Z, Kim H, Liu W, Cong W, Jiang Q, Zhang H. Influence of energy density on macro/microstructures and mechanical properties of as-deposited Inconel 718 parts fabricated by laser engineered net shaping. JManufProcess 2019;42:96–105.
[24] Liu Z, Wang X, Wuest T, Zhang HC. Modeling and experimental analysis of energy attenuation and partitioning during laser based direct energy deposition. Procedia Manuf 2020;48:656–62.
[25] Tolochko NK, Khlopkov YV, Mozzharov SE, Ignatiev MB, Laoui T, Titov VI. Absorptance of powder materials suitable for laser sintering. Rapid PrototypJ 2000;6(3):155–61.
[26] Trapp J, Rubenchik AM, Guss G, Matthews MJ. In situ absorptivity measurements of metallic powders during laser powder-bed fusion additive manufacturing. Appl Mater Today 2017;9:341–9.
[27] Matthews MJ, Guss G, Khairallah SA, Rubenchik AM, Depond PJ, King WE. Denudation of metal powder layers in laser powder bed fusion processes. Acta Mater 2016;114:33–42.
[28] Yang Y, Gu D, Dai D, Ma C. Laser energy absorption behavior of powder particles using ray tracing method during selective laser melting additive manufacturing of aluminum alloy. MaterDes 2018;143:12–9.
[29] Boley CD, Khairallah SA, Rubenchik AM. Calculation of laser absorption by metal powders in additive manufacturing. Appl Optics 2015;54(9):2477.
[30] Gu D, Yang Y, Xi L, Yang J, Xia M. Laser absorption behavior of randomly packed powder-bed during selective laser melting of SiC and TiB2 reinforced Al matrix composites. OptLaser Technol 2019;119:105600.
[31] Liu Z, Zhang HC, Peng S, Kim H, Du D, Cong W. Analytical modeling and experimental validation of powder stream distribution during direct energy deposition. Addit Manuf 2019;30:100848.
[32] Huang YL, Liu J, Ma NH, Li JG. Three-dimensional analytical model on laser-powder interaction during laser cladding. J Laser Appl 2006;18(1):42–6.
[33] Pinkerton AJ. An analytical model of beam attenuation and powder heating during coaxial laser direct metal deposition. J Phys D Appl Phys 2007;40(23):7323.
[34] Liu Z, Li T, Ning F, Cong W, Kim H, Jiang Q, Zhang H. Effects of deposition variables on molten pool temperature during laser engineered net shaping of Inconel 718 superalloy. IntJAdvManufTechnol 2019;102(1–4):969–76.
[35] Kieruj P, Przestacki D, Chwalczuk T. Determination of emissivity coefficient of heat-resistant super alloys and cemented carbide. ArchMechTechnolMater 2016;36(1):30–4.
[36] Kizaki Y, Azuma H, Yamazaki S, Sugimoto H, Takagi S. Phenomenological studies in laser cladding. Part I. Time-resolved measurements of the absorptivity of metal powder. Jpn J Appl Phys 1993;32(1R):205.
[37] Jin S, He X, Wu Y, Ning W, Yu G. Laser power attenuation by powder flow in coaxial laser cladding. ChinJLasers 2011;38(9):0903005.
[38] Liu J, Li L, Zhang Y, Xie X. Attenuation of laser power of a focused Gaussian beam during interaction between a laser and powder in coaxial laser cladding. J Phys D Appl Phys 2005;38(10):1546.
[39] Picasso M, Marsden CF, Wagniere JD, Frenk A, Rappaz M. A simple but realistic model for laser cladding. MetallMaterTransB 1994;25(2):281–91.
[40] Neto ODOD, Vilar RMCDS. Interaction between the laser beam and the powder jet in blown powder laser alloying and cladding. In: International Congress on Applications of Lasers & Electro-Optics. Vol. 1998. Laser Institute of America; 1998, November. D180–8. No. 1.
[41] Miotello A, Kelly R. Laser-induced phase explosion: new physical problems when a condensed phase approaches the thermodynamic critical temperature. Appl Phys Mater Sci Process 1999;(S1):S67–73.
[42] Leitz KH, Redlingshöfer B, Reg Y, Otto A, Schmidt M. Metal ablation with short and ultrashort laser pulses. PhysProcedia 2011;12:230–8.
[43] Mannion P, Magee J, Coyne E, O'Connor G, Glynn T. The effect of damage accumulation behaviour on ablation thresholds and damage morphology in ultrafast laser micro-machining of common metals in air. Appl Surf Sci 2004;233(1–4):275–87.
[44] Ullsperger T, Liu D, Yürekli B, Matthäus G, Schade L, Seyfarth B, Kohl H, Ramm R, Rettenmayr M, Nolte S. Ultra-short pulsed laser powder bed fusion of Al-Si alloys: impact of pulse duration and energy in comparison to continuous wave excitation. Addit Manuf 2021;46:102085.
[45] Orosco J, Coimbra CFM. Anomalous carrier transport model for broadband infrared absorption in metals. PhysRevB 2018;98(23):235118.
[46] Hipp D, Mahrle A, Beyer E. Beyond Fresnel: absorption of fibre laser radiation on rough stainless steel surfaces. J Phys D Appl Phys 2019;52(35):355302.
[47] Boley CD, Khairallah SA, Rubenchik AM. Calculation of laser absorption by metal powders in additive manufacturing. Appl Optics 2015;54(9):2477–82.
[48] Brandau B, Da Silva A, Wilsnack C, Brueckner F, Kaplan AF. Absorbance study of powder conditions for laser additive manufacturing. MaterDes 2022;216:110591.
[49] Cheng Y, Jin X, Li S, Zeng L. Fresnel absorption and inverse bremsstrahlung absorption in an actual 3D keyhole during deep penetration CO2 laser welding of aluminum 6016. OptLaser Technol 2012;44(5):1426–36.
[50] Sharifian M, Ghoveisi F, Firouzi Farrashbandi N. Inverse Bremsstrahlung absorption in under-dense plasma with Kappa distributed electrons. AIP Adv 2017;7(5):055107.
[51] Kundu M. Collisional absorption of laser light in under-dense plasma: the role of Coulomb logarithm. PhysPlasmas 2014;21(1):013302.